Volumetric scans of wind turbine wakes performed with three simultaneous wind LiDARs under different atmospheric stability regimes

Giacomo Valerio Iungo and Fernando Porté-Agel

Wind Engineering and Renewable Energy Laboratory (WIRE), École Polytechnique Fédérale de Lausanne (EPFL), Station 2, 1015, Lausanne, Switzerland.

E-mail: valerio.iungo@epfl.ch

Abstract. Aerodynamic optimization of wind farm layout is a crucial task to reduce wake effects on downstream wind turbines, thus to maximize wind power harvesting. However, downstream evolution and recovery of wind turbine wakes are strongly affected by the characteristics of the incoming atmospheric boundary layer (ABL) flow, such as wind shear and turbulence intensity, which are in turn affected by the ABL thermal stability. In order to characterize the downstream evolution of wakes produced by full-scale wind turbines under different atmospheric conditions, wind velocity measurements were performed with three wind LiDARs. The volumetric scans are performed by continuously sweeping azimuthal and elevation angles of the LiDARs in order to cover a 3D volume that includes the wind turbine wake. The minimum wake velocity deficit is then evaluated as a function of the downstream location for different atmospheric conditions. It is observed that the ABL thermal stability has a significant effect on the wake evolution, and the wake recovers faster under convective conditions.

1. Introduction

Recent national energy reports show wind energy as the fastest growing non-hydro renewable energy source. However, wind farm productivity, which is characterized through the capacity factor, is reaching asymptotic values for different sites, even with an increasing number of installed turbines [1]. This limitation on wind power harvesting from a wind farm is mainly ascribed to interactions of wind turbine wakes within wind farms, as documented in [2] and [3]. Turbine wakes are the result of an energy transformation process, indeed a percentage of the kinetic energy of the incoming wind is converted in rotational momentum connected to the rotation of the turbine blades, and in turn in electricity. The result of this energy transformation process is the presence of a significant velocity deficit just downstream of the turbine, i.e. the turbine wake, which gradually recovers to the incoming wind velocity field by moving downstream. The wake recovery is mainly due to the flow entrainment from the atmospheric boundary layer (ABL) flow into the wake. The wake flow is also characterized by a significant turbulence, which is mechanically produced from the turbine rotation and the consequent velocity deficit. Wake turbulence can represent a hazard for downstream turbines due to enhanced fatigue loads.

The morphology of wind turbine wakes and their mutual interactions within a wind farm, are affected by the ABL characteristics. Indeed, wind turbines are immersed in a region of the

ABL characterized by different levels of shear, stratification and turbulence, which vary on daily and seasonal cycles [4]. Wind characteristics change with the thermal stability regime of the ABL, which can be classified as stable, neutral and convective. A convective ABL is typically observed onshore during day time, when the terrain is heated by the sun. Under ABL convective conditions, heat transfer between the terrain and the air produces positive buoyancy, which leads to increased turbulence levels [5]. On the other hand, a stable ABL is typically observed during night time, and it is characterized by reduced turbulence levels and a significant wind shear. Finally, a neutral ABL represents a transitional regime between convective and stable regimes, and vice versa. For a neutral ABL the mean potential temperature gradient is negligible and turbulence is mainly mechanically produced by shear in proximity of the terrain.

Several studies have shown that ABL stability can affect noticeably power harvesting [6, 7, 8, 9]. For investigations of full-scale turbines presented in [10], a larger power harvesting was observed under stable ABL conditions, compared with neutral conditions. This result is in agreement with the work presented in [11], which reports a lower power production from a single turbine operating in a convective ABL, compared with stable conditions.

Regarding the effects of ABL stability on the downstream evolution of wind turbine wakes, in [12] wake measurements performed with kite anemometry behind a 2.5 MW wind turbine showed a slower wake recovery for stable regimes, characterized by relatively lower turbulence levels. Recently wind tunnel tests of down-scaled wind turbine models immersed in a convective or neutral ABL were presented in [13]. It was found that the enhanced turbulence, associated with positive buoyancy under convective conditions, leads to a larger flow entrainment and, thus, a faster wake recovery rate.

The wake velocity field produced by a full-scale wind turbine can be evaluated via wind Light Detection and Ranging (LiDAR), see e.g. [14, 15, 16]. In this paper, wind LiDAR measurements of the wake produced by an Enercon E-70 2MW wind turbine under different atmospheric conditions are presented. Wake measurements were performed simultaneously with three scanning Doppler wind LiDARs. One LiDAR was devoted to the characterization of the incoming wind over the rotor disc, while the other two LiDARs performed wind velocity measurements of the wind turbine wake through volumetric scans. The characteristics of the incoming wind were also monitored with a sonic anemometer installed on a 3 m tripod, which was located in proximity of the wind turbine.

The variability in the downstream evolution of wind turbine wake is analyzed for different ABL conditions, and in particular for different ABL stability regimes. The minimum wake velocity deficit is evaluated as a function of the downstream location, then it is fitted through a power law, whose exponent is considered to be a good parameter for the evaluation of the recovery rate of the wake velocity deficit. The paper is organized as follows: the tested wind turbine, the site and the used LiDARs are described in section 2. Measurements for the characterization of the incoming wind field and ABL stability are then reported in section 3. Volumetric scans of the wind turbine wake and analysis of the wake recovery under different ABL stability regimes are provided in section 4. Finally, conclusions are drawn in section 5.

2. Setup

The field campaign was carried out during the period between June and October 2012. The tested wind turbine is an Enercon E-70, with a rotor diameter, d, of 71 m, and hub height, H, of 98 m; its maximum capacity is 2.3 MW. This wind turbine is located in Collonges, Switzerland, within a relatively narrow flat valley bottom about 1 km wide in the Valais region, and it is surrounded by mountains with heights around 2500 m. The wind direction with highest incidence is at 340° from North, which typically occurs during afternoons. It is a thermal wind blowing from the warmer area of the Lake Geneva towards the Alps and is mainly canalized along the valley. The other typical wind has roughly opposite direction, i.e. SSE 160° from North; it

typically blows early in the morning and is commonly slightly stronger than the northerly wind.

Wind velocity measurements were performed simultaneously with three Streamline wind LiDARs, produced by Halo Photonics. These LiDARs emit wave trains with a wavelength of 1.5 μm at a frequency of 15 kHz. They are of the scanning type, i.e. the laser beam direction is fully controlled by the user by setting different values of the azimuth and elevation angles of the laser beam. The highest spatial resolution of the Streamline LiDAR is 18 m, i.e. velocity measurements can be acquired at points evenly spaced along the laser beam with a distance of 18 m. The first available measurement point is at a distance of 45 m from the LiDAR location and the maximum range is about 3 km. The maximum sampling frequency is 0.77 Hz.

The ABL stability is characterized through the evaluation of the Obukhov length, L, which requires single-point heat flux measurements in the surface layer. These measurements were performed with a Campbell Scientific CSAT3 sonic anemometer, which was installed on a tripod at a height of 3 m in proximity of the turbine location. Specifically, it was placed at a transversal distance of about 100 m, in order to avoid any effect of the wind turbine on the measurements. Wind velocity and temperature data were acquired with a sampling frequency of 20 Hz during the entire testing period.

The wind turbine location and the chosen LiDAR locations were determined through a GPS system. Moreover, azimuthal displacements of the LiDAR laser beam, needed to reach the measurement targets, were also evaluated through the GPS. The used GPS is the GRS-1 by TOPCON, which works with GPS and GLONASS receivers. This GPS can achieve a precision of 300 mm with DGPS network.

The reference frame used for this field campaign has its origin at the base of the wind turbine tower. The x-axis corresponds to the mean wind direction, positive in the downstream direction. The mean wind direction was evaluated for three different time periods: the sampling period of each volumetric scan, 5-minute periods and 10-minute periods. The z-axis is along the vertical direction, positive upwards, while y-axis is along the spanwise direction, oriented in a way to produce a right-handed Cartesian coordinate system. A supplementary reference frame was used for the post-processing of the LiDAR data; its x'-axis corresponds to the line connecting the turbine location and the LiDARs deployed downstream of the turbine, the z-axis is unchanged, and the y'-axis is along the spanwise direction, oriented in a way to produce a right-handed Cartesian coordinate system. More details about the experimental setup and the tested wind turbine can be found in [15].

3. Characterization of incoming wind flow

The incoming wind conditions were monitored through one wind LiDAR located at a distance of $12d$ upwind of the wind turbine location. This LiDAR performed staring measurements by setting the azimuthal angle of the LiDAR laser beam in the mean wind direction and the elevation angle at 7.8°, in order to reach the turbine hub height at a distance of $2d$ upwind from the turbine location. This location was used to evaluate the reference wind velocity at hub height, U_{hub}. By assuming that the azimuthal angle of the LiDAR laser beam is perfectly aligned with the mean wind direction, a good approximation of the horizontal velocity is simply obtained by considering that the LiDAR radial velocity is the projection of the horizontal velocity over the laser beam direction. The LiDAR staring measurements were carried out with the maximum sampling frequency of 0.77 Hz, in order to characterize not only the evolution of the mean wind velocity, but also wind velocity fluctuations [14, 15].

The mean vertical profile of the incoming wind was characterized with the dimensionless wind shear exponent, α, through the following power law:

$$U(z) = U_R \left(\frac{z}{z_R} \right)^{\alpha}, \tag{1}$$

where $U(z)$ is the mean horizontal wind speed measured at height z, while U_R is a reference velocity measured at a height typically very close to the ground, z_R. The fitting of the wind measurements was performed by considering heights within the range $-1 < (z - H)/d < 1$. A stable ABL regime is typically characterized by the presence of a significantly sheared flow, which is generally associated to $\alpha > 0.2$. Conversely, a convective ABL regime is characterized by relatively uniform wind velocities along the vertical direction, thus $\alpha < 0.1$. Finally, a neutral ABL regime is characterized by $0.1 < \alpha < 0.2$, see e.g. [17, 18].

The ABL stability was characterized through the evaluation of the Obukhov length, L, which is an indicator of atmospheric mixing conditions in the surface layer following the Monin-Obukhov similarity theory [5]. The Obukhov length is calculated as follows:

$$L = -\frac{\theta_v \cdot u_*^3}{k \cdot g \cdot \overline{w'\theta'_v}}; \tag{2}$$

where θ_v is the virtual potential temperature (in K), k is the von Karman constant (0.4), g is the gravitational acceleration, $\overline{w'\theta'_v}$ is the surface heat flux, and u_* is the friction velocity calculated as $u_* = (\overline{u'v'}^2 + \overline{v'w'}^2)^{1/4}$. Negative values of L are obtained for convective ABL regimes, whereas positive L values correspond to stable ABL regimes. For practical applications, the ABL is often considered stable for 0 m $< L <$ 200 m, whereas it is convective for -300 m $< L <$ 0 m (see e.g. [11]). For smaller or larger L the ABL is considered as neutral. For this site, during the testing period a transition from neutral to convective conditions was typically observed around 10h00 local standard time (LST), while a transition from convective to neutral ABL regimes occurred at around 17h00 LST. Unfortunately, a stable ABL was never observed during the testing period.

For this study, measurements carried out on October 8, 2012 are considered. That day, transition between the convective and neutral ABL regimes was observed two times during the afternoon. For the characterization of the incoming wind, statistics were performed over different types of time periods. In particular, key flow parameters were calculated for each volumetric scan (i.e. for a time period of 110 s), as well as over 5-minute and 10-minute periods, and the results are reported in Fig. 1. For the total duration of the measurements considered here, the mean incoming wind velocity at hub height, U_{hub}, evolved from 9 to 4 ms^{-1} (Fig. 1a).

The Obukhov lenght, L, reported in Fig. 1b, clearly highlights that for the chosen testing period the ABL was convective around 16 h LST and a transition to neutral occurred around 16.2 h LST (decimal time) due to an overcast. Then, the ABL turned back to convective at 16.6 h LST, and became finally neutral around 17h LST, because of the reduced solar radiation in the late afternoon.

Besides the mean wind velocity, the incoming wind is also characterized through the evaluation of the dimensionless shear exponent, α, defined in Eq. 1, and the turbulence intensity, which are plotted in Figs. 1c and 1d, respectively, while their statistics are reported in Table 1. For the tests performed during an ABL convective regime, i.e. with -300 m $< L <$ 0 m, α had a noticeable variability and a mean value of 0.14. A similar mean α value (0.16) was observed for the neutral ABL regime. Regarding wind turbulence intensity at hub height, which is equal to the ratio between standard deviation and mean value of the velocity as percentage, a mean value of 10.3% was obtained for ABL convective conditions, whereas 9.4% was found for neutral conditions. These results indicate that wind shear and turbulence intensity of the incoming wind at the turbine hub height are only weakly influenced by ABL stability. Therefore, the incoming wind at the rotor height is above the ABL surface layer, and it is likely to be influenced by the steep topography that surrounds the valley, where the turbine is placed.

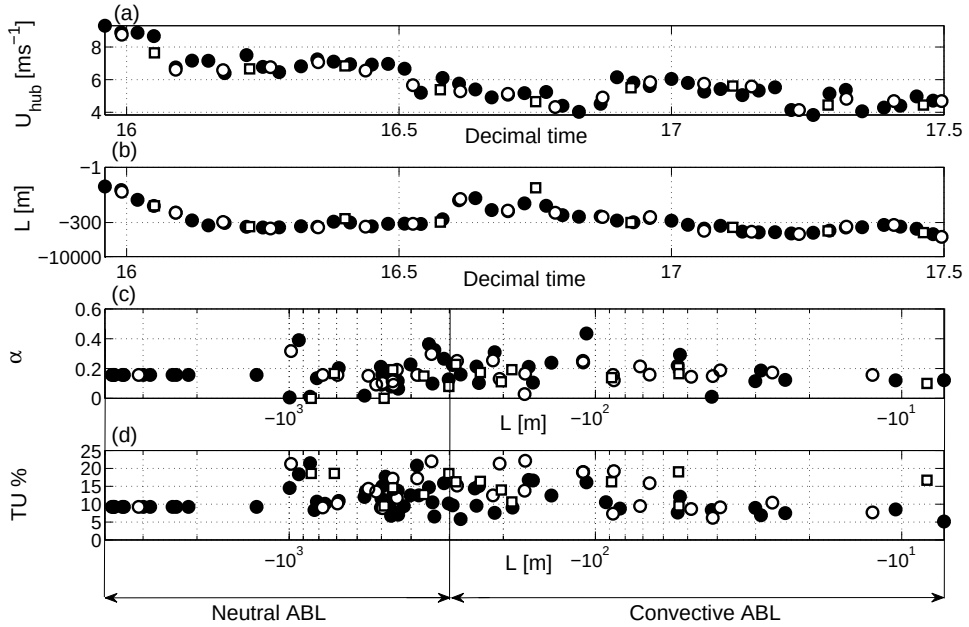

Figure 1. Characterization of the incoming wind: (a) hub height velocity, U_{hub}; (b) surface-layer Obukhov lenght, L; (c) dimensionless wind shear exponent, α; (d) wind turbulence intensity at hub height. (Symbols represent statistics performed over different time periods: black circle, single volumetric scan (110s); white circle, 5 minutes; white square, 10 minutes).

Table 1. Statistics of the incoming wind for different ABL stability regimes: (left-hand-side) dimensionless wind shear exponent, α; (right-hand-side) turbulence intensity at hub height.

Dimensionless wind shear exponent, α		
	Convective ABL	Neutral ABL
Mean	0.14	0.16
Median	0.13	0.17
Maximum	0.44	0.39
Minimum	0.01	0.01
St. Dev.	0.13	0.13

Turbulence intensity at hub height		
	Convective ABL	Neutral ABL
Mean	10.3%	9.4%
Median	9.3%	9.7%
Maximum	22%	21.5%
Minimum	5.1%	6.5%
St. Dev.	3.4%	3.6%

4. 3D characterization of the wake velocity field

The wake velocity field was measured through volumetric scans, which were carried out by sweeping both elevation and azimuthal angles of the LiDAR laser beam, in particular the azimuthal angle within a range of 20°, centered with the wind turbine hub and with angular steps of 2°, while the elevation angle was varied from 2° up to 16° with an angular step of 2°. In order to reduce the sampling period required for each volumetric scan, measurements were performed simultaneously with two LiDARs, and each LiDAR measured over half measurement volume. With this procedure a sampling period of 110 s per scan was obtained.

A typical wake velocity field measured through a volumetric scan is reported in Fig. 2. For these tests the two LiDARs were deployed at the downstream location $x'/d = 12$. In Fig. 2 transversal planes are reported for different downstream locations, which allow the characterization of the wind turbine wake over different cross-sections. In particular, the morphology of the wake can be clearly observed, with its location and wake velocity deficit.

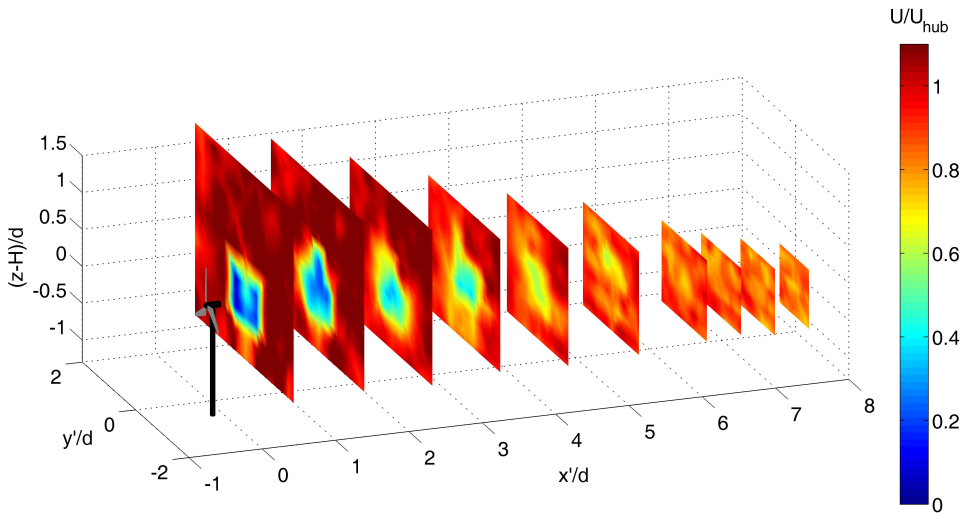

Figure 2. Velocity field obtained through a volumetric scan. Transversal planes at different downstream locations ($x/d = 0.6; 1; 2; 3; 4; 5; 6; 7; 7.6; 8$).

The evaluation of the velocity field over the horizontal plane located at hub height, which is reported in Fig. 3a, allows a more detailed characterization of the wake recovery. Indeed, this figure shows that the strong velocity deficit observed in the near-wake region gradually recovers moving downstream, while a slight increase of the wake width is also observed, especially for distances $x/d > 3$.

In Fig. 3a the wake vertical symmetry plane, which is the vertical plane passing through the turbine location and parallel to the mean wind direction, is represented with a black line. For the considered test, it is rotated 2° counter-clockwise from the x'-axis. Subsequently, the wind velocity field is also evaluated over the wake vertical symmetry plane, as reported in Fig. 3b, showing the wake velocity deficit and the wake recovery.

Through the detection of the wake vertical symmetry plane, a new reference frame can be defined by rotating the existing one around the z-axis, in order to obtain the $x-z$ plane coincident with the wake vertical symmetry plane. The velocity field evaluated for the new reference frame is characterized by only one non-negligible component, which is the one oriented along the x-axis and referred to as axial velocity. This is a reliable assumption for wind turbine wake flows, except for the very near wake ($x/d < 1$) where a small transversal velocity component could be present due to wake swirl [15, 19, 20]. Therefore, for each scan an approximated axial velocity is evaluated by considering that the radial velocity is the projection of the axial velocity over the respective LiDAR laser beam direction [14].

Averaged velocity fields were also calculated from several volumetric scans in order to characterize the wake recovery over longer sampling periods. This procedure allows the enhancement of the statistical stationarity of the parameters evaluated for the characterization of the wake recovery. Generally the mean radial velocity field was calculated from three consecutive scans, thus for a sampling period of 330 s, with the constraints of a maximum difference between the three considered scans of 1 ms^{-1} for U_{hub} and 2° for the mean wind direction.

The wake velocity deficit and its downstream recovery are analysed with two different methods, i.e. by selecting for each downwind distance the minimum value of the axial velocity over a transversal plane, and over its intersection with the wake vertical symmetry plane. For the volumetric scan presented in Figs. 2 and 3, the evolution of the wake velocity deficit is shown in Fig. 4; it is evident that the two criteria are in good agreement for the evaluation of

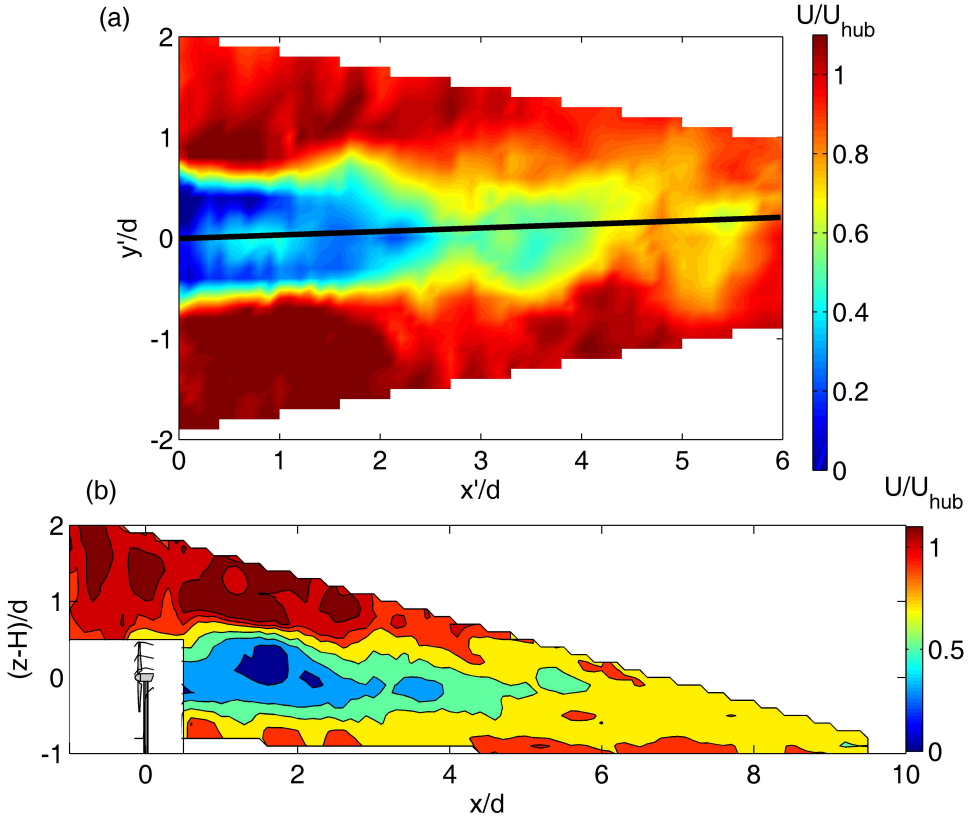

Figure 3. Velocity field obtained through a volumetric scan: (a) section over the horizontal plane at hub height (vertical simmetry plane of the wake highlighted with a black line); (b) section over the wake vertical symmetry plane.

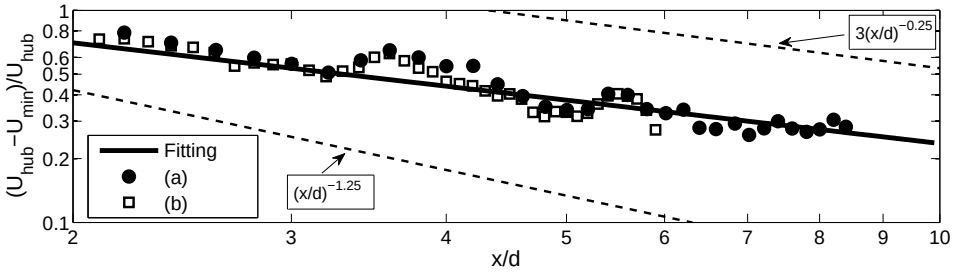

Figure 4. Velocity field obtained through a volumetric scan: velocity deficit as a function of the downstream location evaluated through two methods: (a) black circle, as minimum of the axial velocity for the different transversal planes; (b) white square, as minimum of the axial velocity over the wake vertical symmetry plane for different downstream locations. The solid black line represents the curve fitting the wake velocity deficit as defined in Eq. 3.

the wake velocity deficit.

In several works, e.g. [3, 13], the downstream recovery of the wake velocity deficit is typically represented by the following power law:

$$\frac{U_{hub} - U_{min}}{U_{hub}} = A \left(\frac{x}{d}\right)^n , \tag{3}$$

where U_{hub} is the reference velocity, which is measured by the LiDAR located upwind for the characterization of the incoming wind. U_{min} is the minimum axial velocity observed at a certain downstream location. The parameter A depends on the turbine characteristics, and it is related to the thrust coefficient, while the exponent n is connected to the rate of wake recovery; a larger n corresponds to a slower wake recovery. From the above-mentioned works, typical values for these coefficients are $A \in [1, 3]$ and $n \in [-1.25, -0.25]$; the two corresponding extreme lines are shown in Fig. 4 as two dashed black lines. In the same figure, the curve fitting corresponding to the considered volumetric scan is reported with a solid black line, which shows that the recovery of the wake velocity deficit can adequately be represented through the law reported in Eq. 3. However, some scattering around the curve fitting is observed due to the turbulent nature of the wind turbine wake flow and to the sampling time of 110 s related to a single volumetric scan.

The fitting coefficients A and n were evaluated for each volumetric scan and also for the mean velocity fields obtained by averaging the wind data from three consecutive scans. The fitting coefficients A and n are reported in Fig. 5 as a function of the Obukhov length, L, i.e. of the ABL stability condition; moreover, their statistics are reported in Tables 2 and 3. For the convective ABL regime the mean value of the coefficient A is 1.46 for the single scans and 1.03 for the averaged data, whereas for the neutral regime its mean value is 0.95 and 0.78 for the single and averaged scans, respectively. Considering that typical values for the coefficient A are included within the interval [1, 3], it appears that ABL stability has only a weak effect on the fitting coefficient A.

The downstream recovery of the wake velocity deficit is then characterized through the fitting coefficient n of Eq. 3. From Fig. 5b it is evident that n is generally increased with decreasing Obukhov length, L, i.e. moving from a convective ABL regime to a neutral one. For the single scans, the mean value of n changes from -0.68 for the convective regime to -0.29 for the neutral one; analogously, for the averaged data, it varies from -0.76 to -0.26. Considering that typical values of n are included within the interval $[-1.25, -0.25]$, it can be concluded that the influence of the ABL stability condition on the wake recovery is remarkable. Specifically, a faster wake recovery is observed for convective ABL regimes. This feature is largely appreciable in Fig. 6, where all the lines obtained through the curve fitting of the downstream evolution of the wake velocity deficit are reported for each volumetric scan. The curves associated to a neutral ABL regime are reported in blue, whereas the ones ascribed to a convective ABL are reported in red. The latter have clearly a higher slope, which is due to a faster recovery of the wake velocity deficit. These results are in good agreement with the wind tunnel experiments performed by [13],

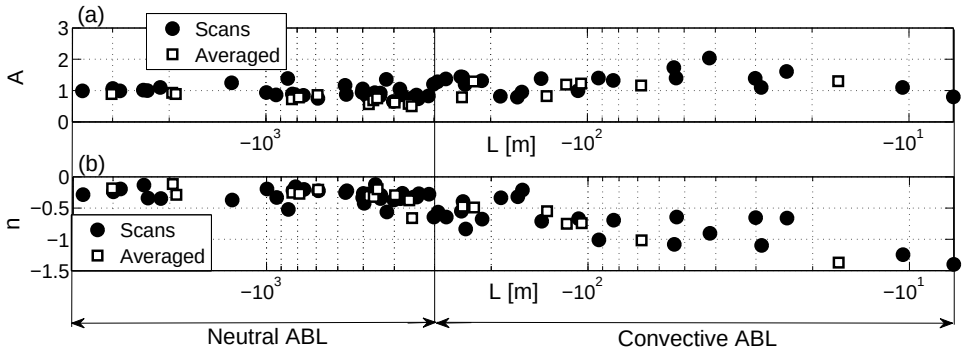

Figure 5. Fitting coefficients of the wake velocity deficit function in Eq. 3 as a function of the Obukhov length, L: (a) fitting coefficient A; (b) fitting coefficient n. (Symbols: black circle, parameters obtained from single volumetric scans; white square, parameters obtained from averages of three consecutive volumetric scans).

Table 2. Statistics of the fitting coefficient A of the wake velocity deficit function defined in Eq. 3, evaluated for different ABL stability conditions and different sampling periods: (left-hand-side) statistics of A calculated from each volumetric scan; (right-hand-side) statistics of A calculated from averaged velocity fields of three consecutive scans.

Single volumetric scans			Averaged velocity fields		
	Convective ABL	Neutral ABL		Convective ABL	Neutral ABL
Mean	1.46	0.95	Mean	1.03	0.78
Median	1.38	0.92	Median	1.18	0.77
Maximum	2.1	1.38	Maximum	1.30	0.98
Minimum	0.78	0.65	Minimum	0.70	0.57
St. Dev.	0.62	0.17	St. Dev.	0.27	0.15

Table 3. Statistics of the fitting coefficient n of the wake velocity deficit function defined in Eq. 3, evaluated for different ABL stability conditions and different sampling periods: (left-hand-side) statistics of n calculated from each volumetric scan; (right-hand-side) statistics of n calculated from averaged velocity fields of three consecutive scans.

Single volumetric scans			Averaged velocity fields		
	Convective ABL	Neutral ABL		Convective ABL	Neutral ABL
Mean	-0.68	-0.29	Mean	-0.76	-0.26
Median	-0.66	-0.28	Median	-0.70	-0.28
Maximum	-0.21	-0.12	Maximum	-0.48	-0.12
Minimum	-1.4	-0.64	Minimum	-1.37	-0.66
St. Dev.	0.27	0.1	St. Dev.	0.15	0.07

for which a relatively faster wake recovery was also observed under convective conditions. The observed variability of the wake recovery rate can be ascribed to an increased turbulence level present within the ABL surface layer under convective conditions, which is likely associated with an increased exchange of momentum and energy between the turbine wake and the surrounding ABL flow. This, in turn, leads to an enhanced flow entrainment within the wake and, thus, to a faster wake recovery.

5. Conclusions

A field campaign was performed in order to investigate the influence of atmospheric conditions on the downstream evolution and recovery of wind turbine wakes. To this aim velocity measurements were simultaneously carried out with three scanning Doppler wind LiDARs. One LiDAR was devoted to the characterization of the incoming wind, in particular mean velocity at hub height, wind shear and wind turbulence intensity. The thermal stability condition of the atmospheric boundary layer (ABL) was characterized through the evaluation of the Obukhov length, which was obtained from single-point heat flux measurements carried out with a sonic anemometer.

The other two LiDARs performed volumetric scans of the wind turbine wake, which resulted to be a very efficient measuring technique for the characterization of wind turbine wake flows. For the wake velocity fields obtained from each volumetric scan and from averages of three consecutive volumetric scans, the wake velocity deficit was evaluated as a function of the downstream location, then fitted through a power law. This analysis shows that the wind

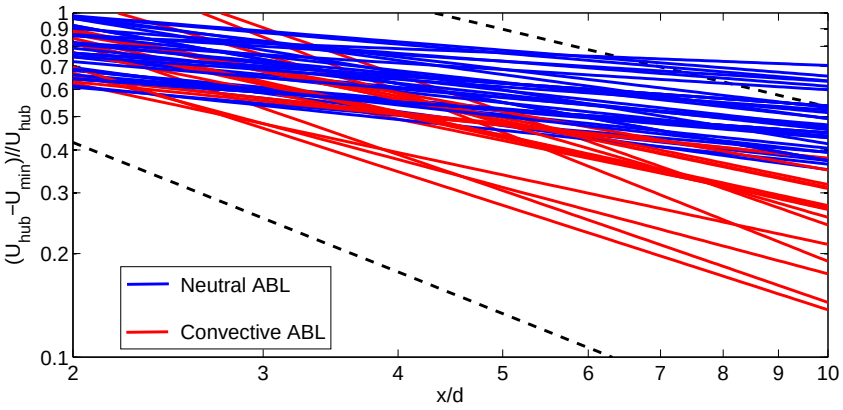

Figure 6. Curve fitting of the wake velocity deficit as a function of the downstream location as defined in Eq. 3. Blue lines are associated to volumetric scans performed under neutral ABL conditions, whereas the red ones were obtained under convective conditions.

turbine wake recovers faster under convective conditions, compared with the neutral ones. This enhanced wake recovery rate is likely related to increased turbulence levels within the ABL surface layer, which promote ABL flow entrainment into the wake.

This noticeable effect of ABL stability on the downstream evolution of wind turbine wakes should be definitely considered for improved wake models, which are essential for numerical simulations of wind turbine wake flows, and for prediction of wind power harvesting. A good comprehension of the variability of wind turbine wakes under different ABL regimes is also crucial for the evaluation of the environmental impact of wind turbine wakes on the local micro-climate. Overall, the field wake measurements presented here provide a valuable dataset for the improvement and validation of numerical models (e.g., analytical models and large-eddy simulations) of wind turbine wakes.

References

[1] Wiser R and Bollinger M 2012 *Tech. rep. Lawrence Berkeley National Laboratory*
[2] Crespo A, Hernandez J and Frandsen S 1999 *Wind Energy* **2** (1) 1-24
[3] Vermeer L J, Sorensen J N and Crespo A 2003 *Prog. in Aerospace Sci.* **39** (6-7) 467-510
[4] Larsen S E, Gryning S E, Jensen N O, Jorgensen H E and Mann J 2007 *Wind Energy, Proc. Euromech Colloquium* Springer Berlin Heidelberg, New York 21-25
[5] Stull R B 1988 *Kluwer Academic*
[6] Elliott D L and Cadogan 1990 *Proc. Europ. Commun. Wind Energy Conf. and Exh.* Madrid, Spain
[7] Motta M, Barthelimie R J and Volund P 2005 *Wind Energy* **8** 219-236
[8] Sumner J and Masson C 2006 *J. Sol. Energy Eng.* **128** 531-537
[9] Gottschall J and Peinke J 2008 *Environ. Res. Lett* **3** 1-7
[10] van der Berg G 2008 *Wind Energy* **11** 151-169
[11] Wharton S and Lundquist J K 2010 *Tech. rep. LLNL-TR-424425*
[12] Baker R and Walker S 1984 *Solar Energy* **33** 5-12
[13] Zhang W, Markfort C D and Porté-Agel F 2013 *Bound. Layer Meteorol.* **146** 161-179
[14] Iungo G V and Porté-Agel F 2013 *Adv. Sci. Res.* **10** 71-75
[15] Iungo G V, Wu Y-T and Porté-Agel F 2013 *J. Atmos. Oceanic Technol.* **30** 274-287
[16] Carbajo-Fuertes F, Iungo G V and Porté-Agel F 2014 *J. Atmos. Oceanic Technol.* in press
[17] Rareshide E, Tindal A, Johnson C, Graves A, Simpson E, Bleeg J, Harris T and Schoborg D 2009 *AWEA WINDPOWER Conf.* Chicago
[18] Wharton S and Lundquist J K 2012 *Wind Energy* **15** 525-546
[19] Iungo G V, Viola F, Camarri S, Porté-Agel F and Gallaire F 2013 *J. Fluid Mech.* **737** 499-526
[20] Viola F, Iungo G V, Camarri S, Porté-Agel F and Gallaire F 2014 *J. Fluid Mech.* in press